JGR Space Physics

RESEARCH ARTICLE
10.1029/2019JA026535

Multi-instrument Observations of Mesoscale Enhancement of Subauroral Polarization Stream Associated With an Injection

Zihan Wang[1], Shasha Zou[1], Simon G. Shepherd[2], Jun Liang[3], Jesper W. Gjerloev[4], J. Michael Ruohoniemi[5], Bharat Kunduri[5], and John R. Wygant[6]

[1]Department of Climate and Space Sciences and Engineering, University of Michigan, Ann Arbor, MI, USA, [2]Thayer School of Engineering, Dartmouth College, Hanover, NH, USA, [3]Department of Physics and Astronomy, University of Calgary, Calgary, Alberta, Canada, [4]Applied Physics Laboratory Johns Hopkins University, Laurel, MD, USA, [5]The Bradley Department of Electrical and Computer Engineering, Virginia Polytechnic Institute and State University, Blacksburg, VA, USA, [6]School of Physics and Astronomy, University of Minnesota, Twin Cities, Minneapolis, MN, USA

Key Points:
- Mesoscale enhancement of SAPS was observed by VAP and SuperDARN on top of the existing large-scale SAPS
- Mesoscale enhancement is associated with energetic ion flux increase, energetic electron flux decrease, and local magnetic field dip
- Mesoscale enhancement of SAPS and equatorward flow burst developed near the Harang reversal

Supporting Information:
- Supporting Information S1

Correspondence to:
Z. Wang,
wzihan@umich.edu

Citation:
Wang, Z., Zou, S., Shepherd, S. G., Liang, J., Gjerloev, J. W., Ruohoniemi, J. M., et al. (2019). Multi-instrument observations of mesoscale enhancement of subauroral polarization stream associated with an injection. *Journal of Geophysical Research: Space Physics*, *124*, 1770–1784. https://doi.org/10.1029/2019JA026535

Received 23 JAN 2019
Accepted 1 MAR 2019
Accepted article online 8 MAR 2019
Published online 25 MAR 2019

Abstract Subauroral polarization streams (SAPS) prefer geomagnetically disturbed conditions and strongly correlate with geomagnetic indexes. However, the temporal evolution of SAPS and its relationship with dynamic and structured ring current and particle injection are still not well understood. In this study, we performed detailed analysis of temporal evolution of SAPS during a moderate storm on 18 May 2013 using conjugate observations of SAPS from the Van Allen Probes (VAP) and the Super Dual Auroral Radar Network (SuperDARN). The large-scale SAPS (LS-SAPS) formed during the main phase of this storm and decayed due to the northward turning of the interplanetary magnetic field. A mesoscale (approximately several hundreds of kilometers zonally) enhancement of SAPS was observed by SuperDARN at 0456 UT. In the conjugate magnetosphere, a large SAPS electric field (~8 mV/m) pointing radially outward, a local magnetic field dip, and a dispersionless ion injection were observed simultaneously by VAP-A at L shell = 3.5 and $MLT = 20$. The particle injection observed by VAP-A is likely associated with the particle injection observed by the Geostationary Operational Environmental Satellite 15 near 20 MLT. Magnetic perturbations observed by the ground magnetometers and flow reversals observed by SuperDARN reveal that this mesoscale enhancement of SAPS developed near the Harang reversal and before the substorm onset. The observed complex signatures in both space and ground can be explained by a two-loop current wedge generated by the perturbed plasma pressure gradient and the diamagnetic effect of the structured ring current following particle injection.

1. Introduction

Subauroral polarization streams (SAPS) refer to high-speed westward convection flows (>100 m/s) in the subauroral ionosphere extending from the afternoon to the early morning sector and can span 3–5° in latitude (Foster & Vo, 2002; Kunduri et al., 2017). In the equatorial magnetosphere, SAPS correspond to large electric fields pointing radially outward from the center of the Earth and are usually observed between the ion and electron plasma sheet inner boundaries and near the plasmapause (e.g., Califf et al., 2016; Kim et al., 2010; Nishimura et al., 2008).

There are a few proposed mechanisms for the formation of SAPS. The current generator theory works as follows (Anderson et al., 1993; Southwood & Wolf, 1978). When the convection increases in the equatorial magnetosphere, a partial ring current can build up on the nightside with large azimuthal pressure gradient. This azimuthal pressure gradient together with the gradient of the magnetic field flux tube volume in the radial direction can generate the Region 2 field-aligned currents (FACs) through $j_{\parallel} \propto [(\nabla V)_{\text{radial}} \times (\nabla P)_{\text{azimuthal}}] \cdot \hat{b}$ (Vasyliunas, 1970). In the above equation, V is the flux tube volume, P is the plasma thermal pressure, and $\hat{b}$ is the direction of the magnetic field. On the duskside, the Region 2 FACs flow into the ionosphere and close through poleward Pederson current and then the Region 1 sense FACs at higher latitudes. When the Region 2 downward FACs are located earthward of the electron plasma sheet inner boundary, where the particle precipitation induced conductance is low, a large poleward electric field, that is, SAPS, in the current closure region is needed to maintain the current continuity. Later, De Keyser (1999) proposed

that the combined effect of finite gyroradius-induced thermoelectric field and the background convection electric field at the front of the substorm particle injection when it reaches the plasmapause can account for the SAPS formation. In addition, Mishin and Puhl-Quinn (2007) pointed out that the short circuiting of the particle injection into the plasmasphere can explain the SAPS formation. According to their theory, when the injected particles enter the plasmapause, energetic electrons will stop, but ions will move further inward. This charge separation will give rise to the SAPS electric field.

Besides the dynamics in the magnetosphere, large convection flow speed and associated enhanced frictional heating in the ionosphere may increase the conversion rate of atomic O^+ to molecular NO^+ and thus increase the recombination rate and plasma loss rate. In addition, enhanced frictional heating leads to elevated ion temperature and ion scale height increase and thus enhanced vertical transport (Heelis et al., 1993). As a result of enhanced frictional heating, the density and conductivity will further decrease, creating a positive feedback effect on the SAPS electric fields (Banks & Yasuhara, 1978; Schunk et al., 1976).

All the above SAPS formation mechanisms suggest that SAPS should occur due to enhanced earthward transport of plasma sheet plasma during geomagnetic active times. Therefore, the SAPS occurrence and characteristics during geomagnetic storms and substorms have been studied extensively using observations. He, Zhang, et al. (2017) show that SAPS occur after 0–1.5 hr after the southward turning of interplanetary magnetic field (IMF) during intense storms. In general, it is found that SAPS move to lower magnetic latitudes and cover larger geomagnetic longitudes as *Kp* increases or *Dst* decreases (Foster & Vo, 2002; Huang & Foster, 2007). The peak SAPS flow speed enhances, and the electron density within the SAPS reduces when *Dst* decreases (Erickson et al., 2011). Recently, Kunduri et al. (2017) showed that the occurrence rate of SAPS can reach over 80% during geomagentic storms ($Dst < -50$ nT). In addition, Wang et al. (2008) also showed that larger cross polar cap potentials are related with larger speed of SAPS, and Anderson (2004) showed that the subauroal potential drop across SAPS is positively correlated with the absolute value of *Dst*. During storm time, a couple of event studies showed that SAPS can last for more than 10 hr (Burke et al., 2000; Califf et al., 2016). This is further confirmed by Lejosne and Mozer (2017) using 2 years of Van Allen Probes (VAP) data and the average lifetime of SAPS was found to be 9 hr, which is comparable to the duration of the storm main phase.

The dynamics of SAPS have been also frequently related to substorms, and it has been shown that they can last from 30 min to 3 hr (Anderson et al., 1991; Makarevich et al., 2009; Puhl-Quinn et al., 2007). Based on the coupled global BATSRUS magnetohydrodynamic model and kinetic ring current model results, SAPS can indeed last for 2–3 hr (Buzulukova et al., 2010; Yu et al., 2015). Although the duration of SAPS and substorm is roughly comparable, we still do not understand the detailed relation between substorm onset and SAPS. Observationally, SAPS have been shown to occur at different phases of a substorm in different cases. Many studies reported that SAPS can form in the expansion and recovery phase, lagging the substorm onset by 6–30 min (Anderson et al., 1993, 2001; Karlsson et al., 1998; Makarevich et al., 2011; Mishin, 2016; Puhl-Quinn et al., 2007; Wang & Lühr, 2011). Anderson et al. (1993) further explained this delay: After the onset, ion and electron plasma sheet boundaries need about 10 min to separate and provide the low conductivity region. However, a much quicker response of SAPS to the onset is later reported, from 30 s after onset (Nishimura et al., 2008) to 2 min (Zou, Lyons, Nicolls, et al., 2009, Zou, Lyons, Wang, et al., 2009). Zou et al. (2012) reported that SAPS can start to form even in the growth phase after the convection starts to increase, as part of the nightside Harang reversal. This is consistent with the current generator theory that SAPS should be able to form following the enhanced convection.

Most studies mentioned above found that SAPS extends over a large spatial scale in the longitudinal direction, covering several hours of magnetic local time (e.g., Clausen et al., 2012; He et al., 2018), and very few studies (Oksavik et al., 2006) focus on mesoscale to small-scale SAPS variations. Recent studies show that small-scale and mesoscale FACs (e.g., Lühr et al., 2015; McGranaghan et al., 2017) and mesoscale flow channels, which are typically associated with streamers and SAPS (Gallardo-Lacourt et al., 2014, 2017), are both important components of the high-latitude ionospheric plasma dynamics. Considering the close relation between SAPS and FACs, it is thus intriguing to study small-scale or mesoscale SAPS variation and the corresponding formation mechanism. In this study, temporal evolution of a SAPS event is investigated using multi-instrument observations from VAP, Super Dual Auroral Radar Network (SuperDARN), Geostationary Operational Environmental Satellite (GOES), and SuperMAG. A mesoscale enhancement of SAPS (MS-SAPS+) extending less than 500 km east-west was observed before a substorm onset. Particle injection,

local magnetic field dip in the equatorial magnetosphere are observed simultaneously with the SAPS electric field. The MS-SAPS+ occurred near the nightside Harang reversal and all phenomena observed by the above mentioned instruments can be explained due to nonsubstorm particle injection and the associated localized pressure enhancement in the equatorial magnetosphere. This paper is organized as follows. Section 2 presents the SAPS event observations from both in situ and ground-based observations. In section 3, the formation mechanism of the mesoscale enhancement of SAPS is discussed and a summary is provided in section 4.

2. Observations

The VAP mission consists of two identically instrumented spacecraft (VAP-A and VAP-B) in nearly identical ~9-hr orbits, with perigee of ~600-km altitude, apogee of 5.8 R_E, and inclination of 10° (Mauk et al., 2014). With the Electric Field and Waves experiment (Wygant et al., 2014) onboard, VAP is an ideal tool to observe the SAPS electric field in the inner magnetosphere. The SAPS event targeted by this paper was observed by VAP-A on 18 May 2013, as shown in Figure 1. The solar wind and IMF conditions during this event are obtained from the National Aeronautics and Space Administration OMNI database and shown in Figure 1a. The IMF Bz was continuously southward except a short excursion to northward between 0445 and 0500 UT. This southward IMF led to a moderate geomagnetic storm with the minimum *SYM-H* reaching −66 nT. This SAPS event occurred during the recovery phase of the storm (the shaded blue area), when the IMF Bz turned back to northward briefly and then southward again.

Figure 1b presents the direct current electric field observed by the Electric Field and Waves instrument in the modified geocentric solar ecliptic (GSE) coordinate (MGSE), which is similar to the GSE coordinates. On the duskside, the E_y component in the MGSE coordinates is pointing approximately duskward (Wygant et al., 2014). Since VAP-A was on the duskside, we can recognize E_y approximately as the radial electric field. A clear electric field enhancement pointing radially outward can be seen with its peak exceeding 8 mV/m at $L = 3.5$ and $MLT = 19.8$ at 0457 UT (indicated by the blue dashed line). This SAPS electric field observation lasted for only 2 min. It is difficult to identify whether this is a spatial or temporal effect based on a single satellite observation. It can be either a small spatial scale structure or a short-lived one. Another possibility is that the spacecraft crossed the edge of the SAPS region and only captured a fraction of it. Figure 1c shows the magnetic field from the Electric and Magnetic Field Instrument Suite and Integrated Science fluxgate magnetometer (Kletzing et al., 2014). A local magnetic dip in the geocentric solar magnetospheric (GSM) Bx and Bz components was encountered by VAP-A at the same time of the SAPS. The electron density derived from the spacecraft potential is shown in Figure 1d. As one can see, SAPS was located slightly earthward of the plasmapause, where the cold electron density suddenly decreased at 0459 UT.

The high energy (50 keV to 1 MeV) spin-averaged ion and electron differential fluxes, shown in Figures 1e and 1f, respectively, are from the Magnetic Electron Ion Spectrometer (MagEIS) instrument (Blake et al., 2014) . A clear dispersionless ion injection (50–200 keV) and an electron flux decrease were observed at about the same time of SAPS. Note that there were jags between different energy channels in the ion flux. However, the amplitude of the jags was small and well within the measurement uncertainty of MagEIS. Figures 1g and 1h present the differential flux of proton and electron from 1 eV to 50 keV from Helium Oxygen Proton Electron (HOPE) mass spectrometer (Funsten et al., 2014). SAPS electric field was located between the inner boundaries of the ion and electron plasma sheets, which means SAPS was located in an ionospheric region with low electron precipitation rate. This low electron precipitation rate may lead to low conductivity in the ionosphere and is a preferred condition to facilitate the SAPS development according to the current generator theory. The perpendicular ion pressure in Figures 1i and 1j were calculated from HOPE and MagEIS, respectively. The pressure from HOPE was calculated using the ion perpendicular temperature and density, while the pressure from MagEIS was calculated using the differential energy flux. Here for simplicity, we assume that the pitch angle distribution (PAD) of particles observed by MagEIS is isotropic. Zhao et al. (2015) show that the isotropic assumption would not significantly influence the magnitude of the pressure. In addition, the gradient of pressure rather the absolute value is more important in the FAC generation theory. At this time, the contribution of electrons to the plasma pressure was much smaller than that of the ions and thus ignored. As one can see, the SAPS electric field was located in the region of large ion pressure gradient. According to the Vasyliunas equation, this pressure gradient, together with the gradient of flux tube volume, gave rise to the Region 2 downward FACs on the duskside (Vasyliunas, 1970), where the conductivity was low due to low electron precipitation shown in Figure 1h. All of these observations

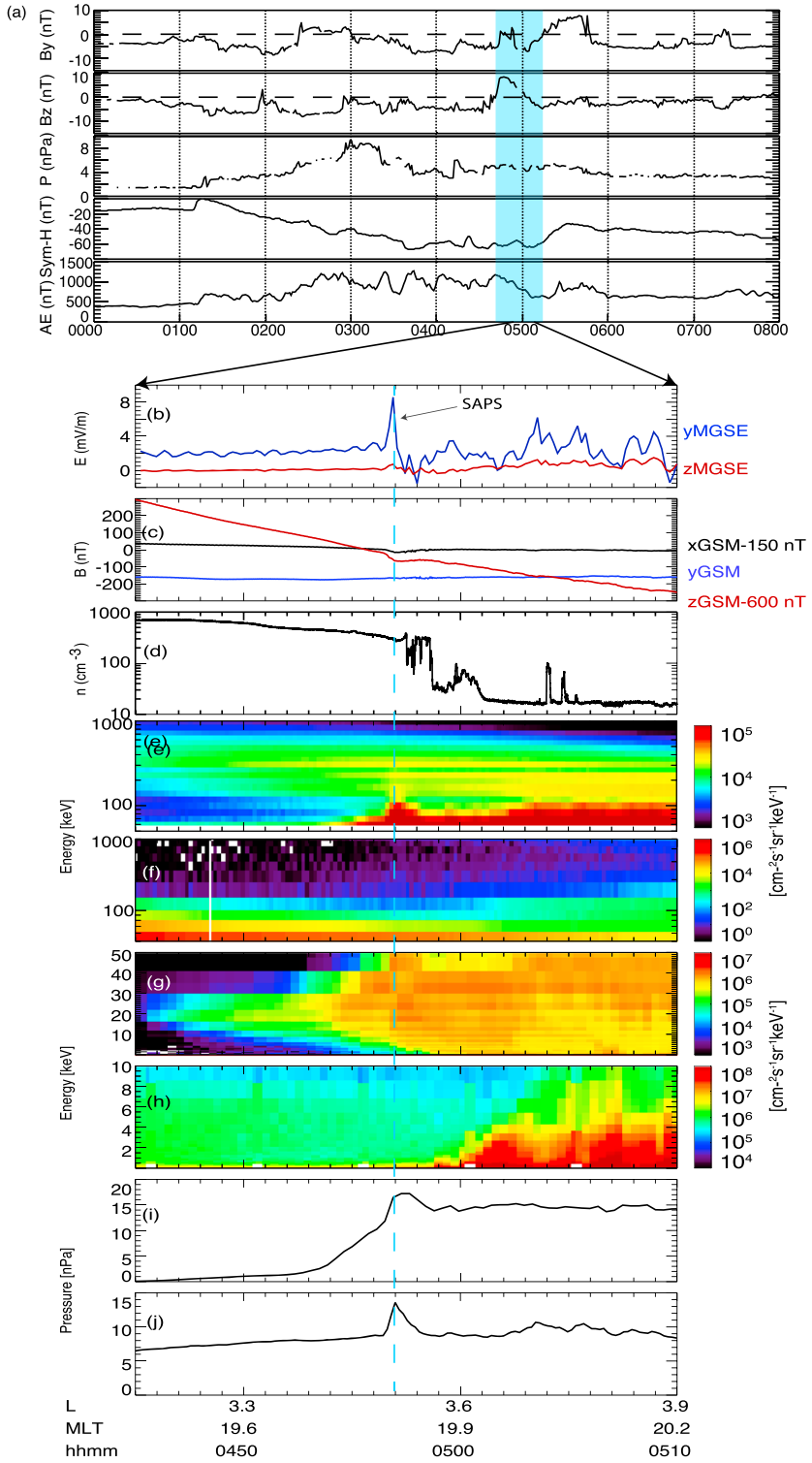

Figure 1. SAPS event on 18 May 2013. (a) Solar wind and geomagnetic data from OMNI. (b) Electric field in the MGSE coordinate from Electric Field and Waves. (c) Magnetic field in GSM coordinate from Electric and Magnetic Field Instrument Suite and Integrated Science. (d) Electron density from the spacecraft potential. (e) Differential ion flux from MagEIS with energy between 50 keV and 1 MeV. (f) Differential electron flux from MagEIS with energy between 50 keV and 1 MeV. (g) Differential proton flux from HOPE with energy below 50 keV. (h) Differential electron flux from HOPE with energy below 10 keV. (i) Perpendicular ion pressure from HOPE. (j) Perpendicular ion pressure from MagEIS. MagEIS = Magnetic Electron Ion Spectrometer; HOPE = Helium Oxygen Proton Electron; MGSE = modified geocentric solar ecliptic; GSM = geocentric solar magnetospheric.

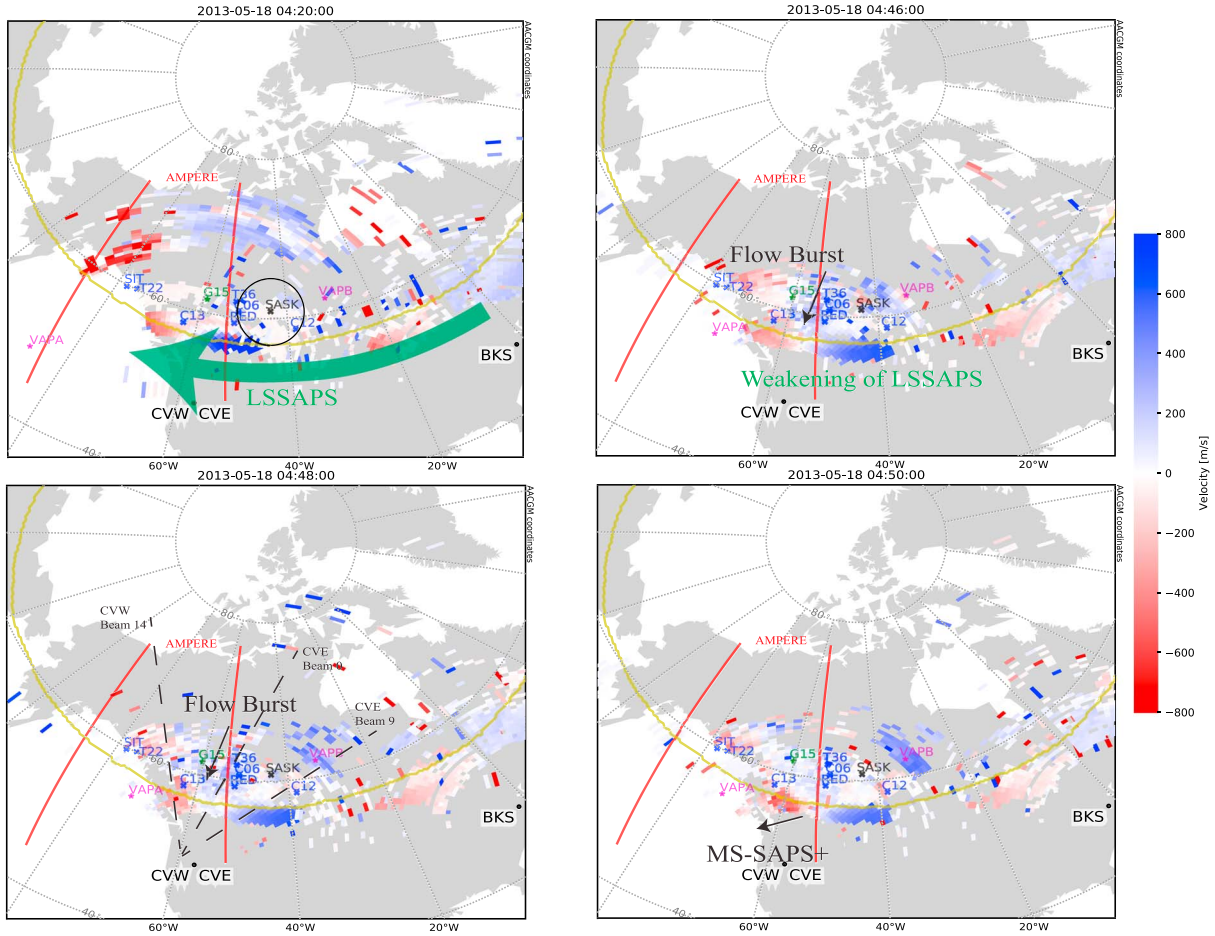

Figure 2. Eight selected maps of the Super Dual Auroral Radar Network line-of-sight velocity in the duskside with ground-based magnetometers, footprints of VAP and GOES, and orbits of AMPERE. Color represents the velocity relative to the radar. Blue means flows are toward the radar, and red means flows are away from the radar. CVW = Christmas Valley West; CVE = Christmas Valley East; BKS = Blackstone; LS-SAPS = large-scale subauroral polarization streams; VAP-A = Van Allen Probes A; VAP-B = Van Allen Probes B; GOES = Geostationary Operational Environmental Satellite.

are consistent with the current generator theory. Note that the electron plasma sheet boundary shown in Figure 1h is dispersive, which is not expected according to the short circuiting theory (Mishin, 2013).

Since observations from one satellite cannot reveal the spatial and temporal variation of the SAPS, it is of vital importance to include the line-of-sight (los) velocity map from SuperDARN in this study. Fortunately, in this event, the footprint of VAP-A was mapped to the west coast of North America, which is well covered by multiple SuperDARN radars. In this study, the los velocity observations from the Christmas Valley West (CVW), Christmas Valley East (CVE), Blackstone (BKS), and Wallops Island (WAL) SuperDARN radars between 4 and 6 UT are considered. Eight selected snapshots of los convection flows are shown in Figures 2 and 3 and a movie of the whole 2-hr period is provided as supporting information. In Figures 2 and 3, the color represents the direction and magnitude of the los velocities with blue representing flows toward the radar and red representing flows away from the radar. Three selected beams, CVW beam 14, CVE beam 0, and CVE beam 9 are indicated by black dashed lines in the panel of 0448 UT, which will be discussed later. The equatorward boundary of the auroral oval, indicated by the yellow dashed line in Figures 2 and 3, is based on the auroral observations centered at 0425 UT and from the Special Sensor Ultraviolet Spectrographic Imager instrument onboard the Defense Meteorological Satellite Program F18. The VAP-A VAP-B and GOES-15 are mapped to the ionosphere based on the Tsyganenko Geomagnetic Field (TS05) model (Tsyganenko & Sitnov, 2005) and are shown as purple (VAP-A and B) and green (GOES15) stars in Figures 2 and 3, respectively. Seven ground-based magnetometers close to the west coast are shown as blue crosses. Two orbital planes of the Iridium satellite near the west coast are also indicated as red lines. As one can see, the footprint of VAP-A was located just equatorward of the Defense Meteorological Satellite Program Special

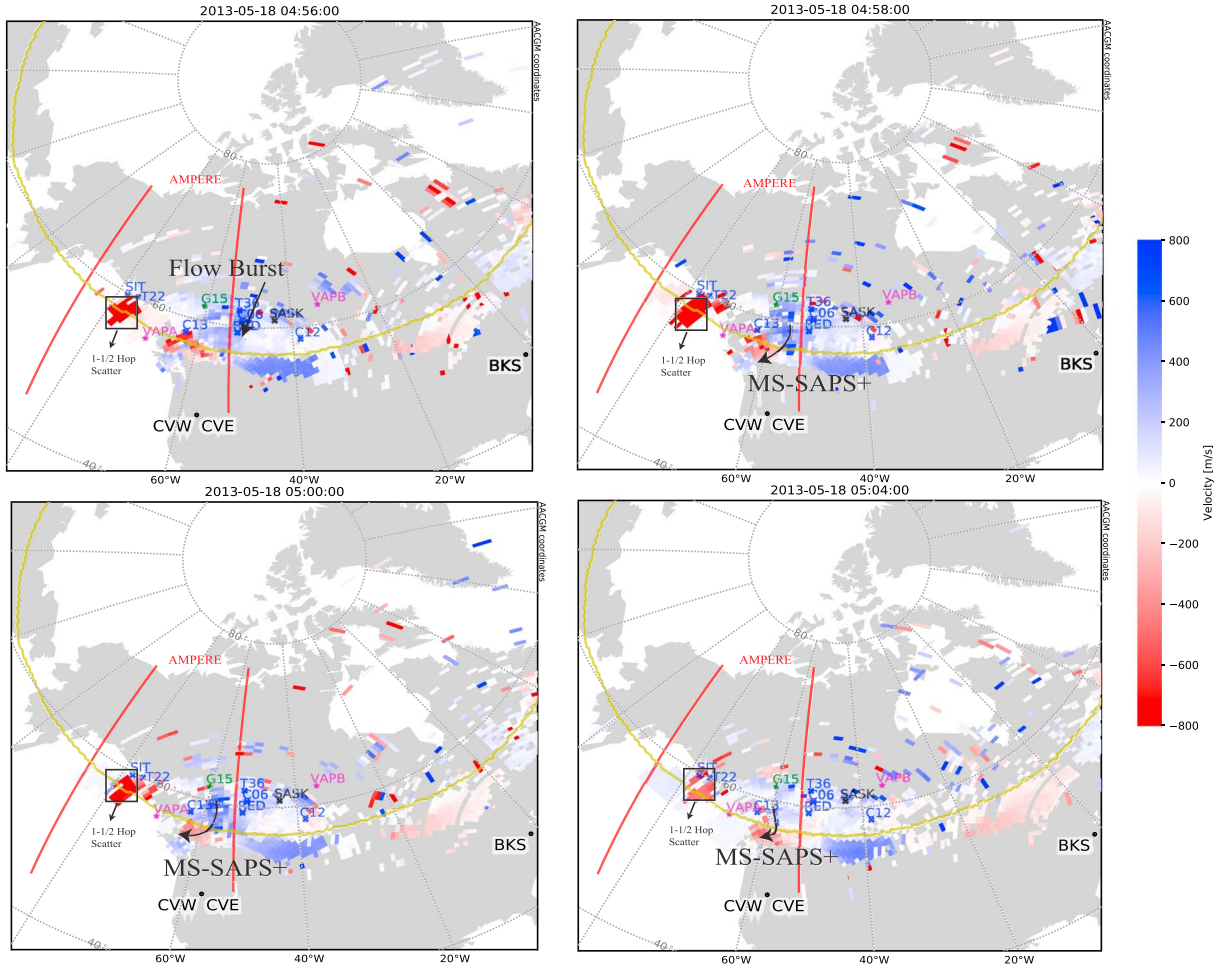

Figure 3. Continued Figure 2.

Sensor Ultraviolet Spectrographic Imager auroral equatorward boundary, which is consistent with the VAP-A observations shown in Figure 1 that the SAPS electric field was earthward of the electron plasma sheet boundary.

As shown in Figure 2, at 0420 UT, in the early recovery phase of the storm, a large-scale SAPS (LS-SAPS) had fully developed and extended across the whole North America continent with peak flow speed exceeding 1,000 m/s. At 0446 UT, when the IMF turned northward, due to the weakening of the convection, the amplitude of the LS-SAPS decreased to ~400 m/s. Another feature is that an equatorward flow, highlighted by a black arrow, occurred poleward of the LS-SAPS and near the footprint of GOES-15 with peak flow amplitude of ~400 m/s. It continued to propagate equatorward at 0448 UT. At 0450 UT, the westward flow near the end of the equatorward flow and near the C13 magnetometer suddenly enhanced to ~600 m/s, while the equatorward flow at higher latitudes disappeared. This SAPS flow enhancement was localized and extended less than 10° in longitude. The eastern part of the LS-SAPS changed little.

In Figure 3, at 0456 UT, another equatorward flow developed near a cluster of magnetometers and again highlighted by a black arrow. At 0458 UT, the equatorward flow moved westward to near the footprint of GOES-15 and sustained the enhancement of westward flow. A very rough estimation of the westward movement of the equatorward flow is 2.5°/min, corresponding an azimuthal velocity of 30 km/s in the geosynchronous orbit. This velocity is comparable with the magnetic drift speed of a 50-keV proton and is consistent with the energy range of the particle injection observed by VAP-A. At 0500 UT, both the equatorward and westward flows began to decrease and at 0504 UT the flow returned back to the background value. Note that the large westward flow near the magnetometers SIT and T22 are 1-1/2 hop scatter, an artificial signal due to the ground scattering. Combining the VAP-A and SuperDARN observations, it is highly

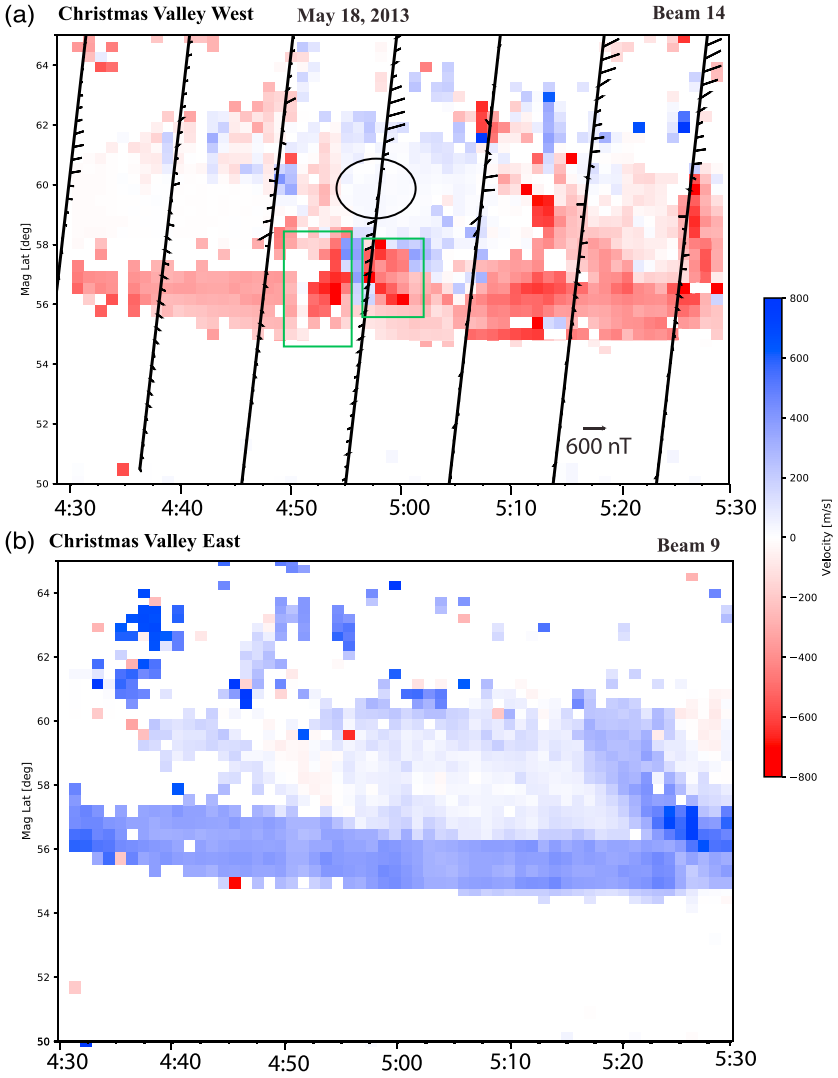

Figure 4. (a) Range-time-intensity (velocity) diagram for the Christmas Valley West beam 14. The red line represents the AMPERE orbital plane in ~20 MLT, and the black arrow represents the vector of the magnetic perturbations. (b) Range-time-intensity (velocity) diagram for the Christmas Valley East beam 9.

likely that VAP-A passed the western edge of this SAPS enhancement region. Considering the spatial scale of this SAPS enhancement is much smaller than the large-scale background SAPS, which extends over several hours of magnetic local time, this SAPS enhancement is thus called a mesoscale enhancement of SAPS (MS-SAPS+).

The los velocity from CVW beam 14, CVE beam 9, and CVE beam 0 are presented in Figures 4 and 5. The looking direction of these three beams is indicated by black dashed lines in Figure 2. The CVW beam 14 and CVE beam 9 together are used to confirm the localization of this SAPS enhancement. Figure 4a shows the los velocity measured by the CVW beam 14 as a function of magnetic latitude and universal time, which is looking westward. The red color indicates that the flows were moving away from the radar, corresponding to westward flows. As one can see, the westward flow was weak before 0450 UT. There were two sudden enhancements at 0450 and 0455 UT, respectively, indicated by green squares, consistent with the two SAPS enhancements following the equatorward flow bursts. Figure 4b is in the same format as Figure 4a but for CVE beam 9, which is looking eastward, and the blue color represents the flow were toward the radar, thus also corresponding to westward flows. The westward flow observed by the CVE beam 9 did not show any enhancement between 0450 and 0500 UT. Therefore, the comparison between the two beams looking at different sections of the LS-SAPS demonstrated that the enhancement of SAPS was localized. Los observa-

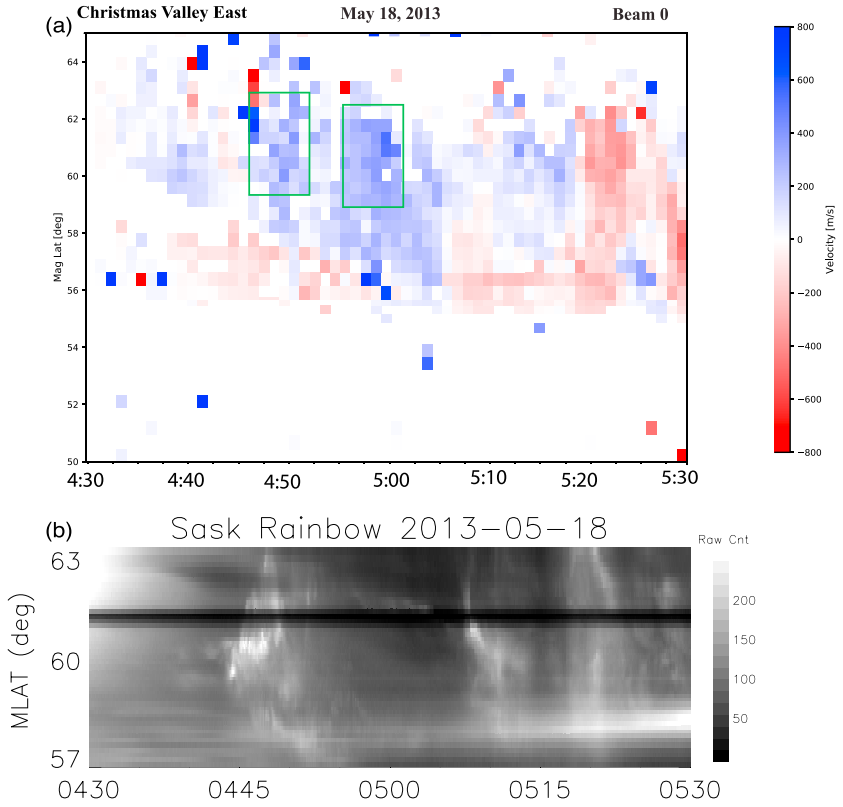

Figure 5. (a) Range-time-intensity (velocity) diagram for the Christmas Valley East beam 0. (b) Keogram fron SASK.

tions from the CVE beam 0 and the keogram from all-sky imager (ASI) at Saskatoon are shown in Figure 5. The keogram is taken at 50°W and check the movie of the ASI measurements in the supporting information. As shown in Figure 2, beam 0 is looking approximately poleward. The blue color represents that the flows are moving mainly toward the radar, corresponding to equatorward flows. The field of view of the ASI is also shown in Figure 2. One can see that the CVE beam 0 is near the western edge of the ASI and it observed both equatorward flow enhancements at 0446 and 0456 UT, respectively. The timing is consistent with that of the westward enhancements at lower latitude in Figure 4a. Although it was cloudy, it still can be seen from the keogram that the aurora activity increased simultaneously with the first flow burst. However, no aurora activity was observed within the Saskatoon ASI during the second flow burst. This is very likely because the flow burst was observed by SuperDARN further to the west and away from the ASI and thus the corresponding aurora activity is out of the scope of the ASI.

The orbital plane of AMPERE near 20 MLT is also presented in Figure 4a, and the black arrows represent the vectors of the magnetic perturbations observed by AMPERE. The vector along the x (y) axis represents the perturbation in the west-east (north-south) direction. The perturbation in the vertical direction is not reflected in Figure 4a. It is shown that when the MS-SAPS+ developed, the magnetic perturbations and the downward FAC were both enhanced. The peak of the downward FAC, where the perturbation changed its direction, is denoted by the black circle. Note that the enhancement later at 0510 UT was related with a substorm onset observed by ground-based ASI (not shown).

During this event, VAP-B, GOES 13, and GOES 15 were also located in the dusk-midnight sector, which can provide large-scale picture about the particle injection activities. Their orbits from 0415 to 0515 UT are shown in Figure 6a. Both VAP-A and GOES-15 were at ~20 MLT, while VAP-B was at ~22 MLT and GOES 13 was right around midnight. The proton and electron fluxes observed by GOES-15 are shown in Figures 6b and 6c, and the magnetic field in GSM coordinate is shown in Figure 6d. Three injections were observed at 0444, 0450, and 0506 UT, respectively, and are indicated by gray arrows. The timing of the first injection is consistent with the first equatorward flow burst at 0446 UT observed by SuperDARN in Figure 2b. Considering the footprint of GOES-15 was very close to the flow channel, both the injection and its manifes-

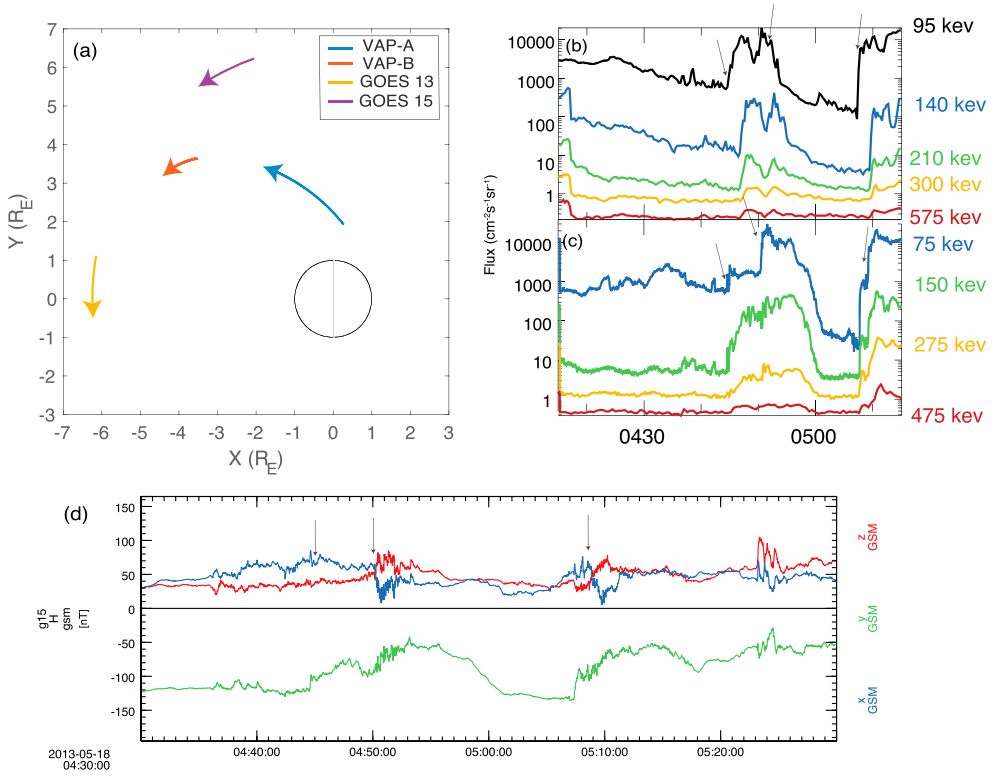

Figure 6. (a) VAP and GOES orbits in the *xy* plane of GSM coordinate. (b) GOES-15 proton flux. (c) GOES-15 electron flux. (d) GOES magnetic field in GSM coordinate. GSM = geocentric solar magnetospheric; VAP = Van Allen Probes; GOES = Geostationary Operational Environmental Satellite.

tation in the ionosphere were thus observed simultaneously. The second injection is likely associated with the SAPS event observed by VAP-A. Considering the conservation of the first adiabatic invariant, the ions of 200-keV energy observed by VAP-A at $L = 3.5$ should have an initial energy around 30 keV at the geosynchronous orbit. Although this energy is lower than the lowest energy of GOES, that is, 95 keV, we can use the arrival time of 95-keV ion to roughly estimate the arrival time of 30 keV in the case of dispersionless injection. Both VAP-B and GOES 13 were on the nightside during this event, but they did not observe any injections. This suggests that the injection was localized and likely from the duskside rather than from the nightside. The radial injection speed is estimated to be ~47 km/s. The velocity is estimated using the positions of two spacecraft and the time difference between the flux increase observed by these two spacecraft. This calculated injection velocity is reasonable (Moore et al., 1981; Reeves et al., 1996) and suggests that the injections observed by VAP-A and GOES-15 are possibly the same one. The third injection was associated with a substorm onset at 0510 UT observed by ground-based ASI and was later than the SAPS event observed by VAP-A.

No magnetic field dipolarization was observed by GOES-15 accompanying the first injection (Figure 6d). After the injection observed by GOES-15, energetic electrons will move eastward due to gradient and curvature drift; thus, it is not likely to be observed by VAP-A that was westward of GOES-15. The second and the third injections were both accompanied by a magnetic dipolarization. This infers that the first injection did not have enough energy to significantly disturb the ambient geomagnetic field at the geosynchronous orbit.

Seven ground magnetometer data obtained from SuperMAG (Gjerloev, 2012) were used to study the magnetic perturbation associated with the SAPS and auroral activities (Figure 7). Daily average was subtracted from the raw data. Their locations relative to the SAPS and auroral boundary are also shown in Figure 2. Negative bays were observed by C12, T36, C06, and RED at 0450 UT. This time is consistent with the time of the MS-SAPS+ (Figure 2). Stations that observed negative bays all located on the east side of the MS-SAPS+. At the same time, positive bays were observed by C13, T22, and SIT, which are close to the MS-SAPS+. Negative (positive) bays are due to enhancement of westward (eastward) auroral currents and thus eastward (west-

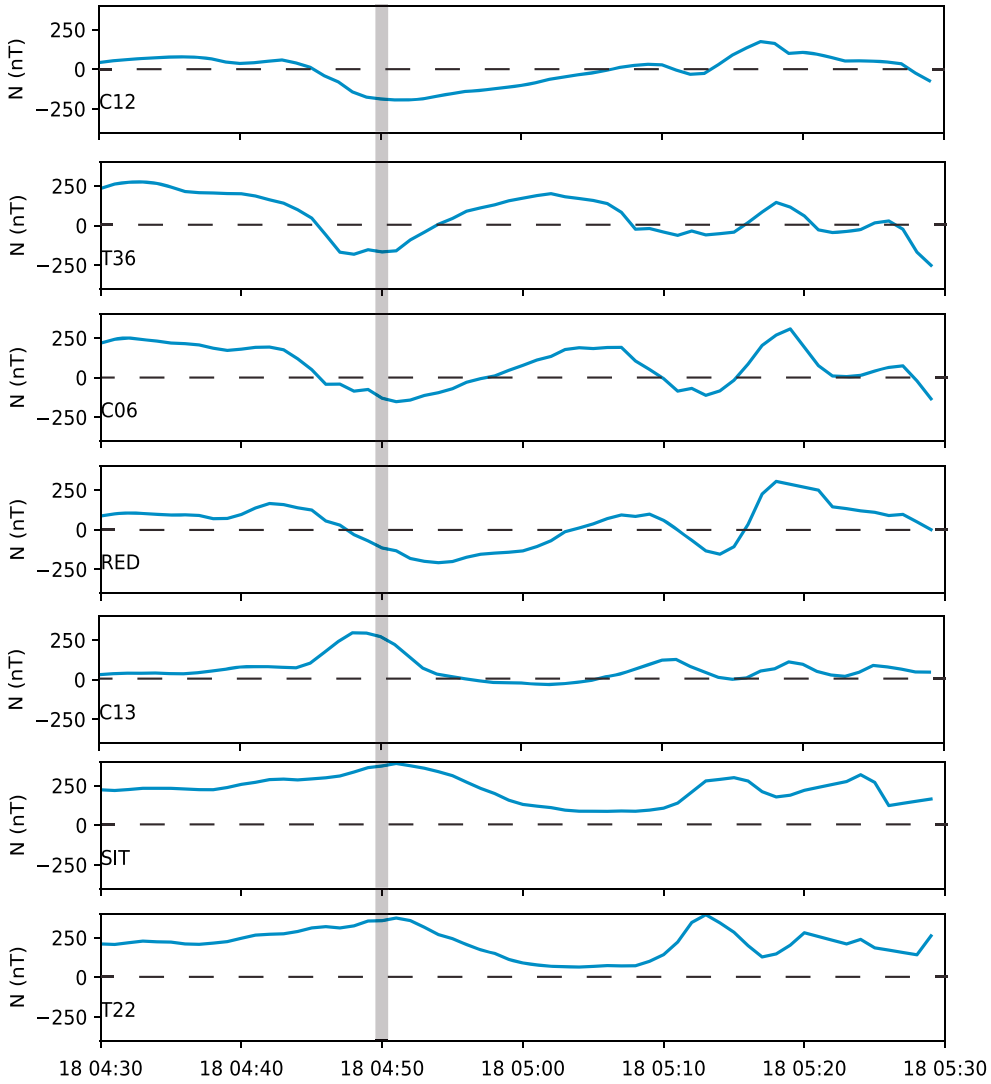

Figure 7. Northward components of the terrestrial magnetic field measured by the ground-based magnetometer stations (taken from SuperMAG).

ward) convection flows. These observations suggest an overlapping of the westward and eastward currents and flows over a narrow latitudinal region comprises the Harang reversal, which can be nicely explained by the schematic plot shown in Figure 8, adapted from Figure 14a in Zou, Lyons, Nicolls, et al. (2009).

In Figure 8, the black curved line represents the equipotential line near the Harang reversal region. VAP-A (magenta star) observed the radially outward electric field, and its footprint is located in the equatorward portion of the Harang reversal. The beams of CVW looking westward observed westward flows. C13, T22, and SIT observed positive magnetic perturbations, due to eastward auroral electrojet and westward convection flows. On the other hand, at the poleward portion of the Harang reversal, negative magnetic perturbations were observed by C12, T36, C06, RED, and equatorward flows were observed by beams looking poleward.

3. Discussion

The SAPS electric field and other complementary measurements from VAP-A presented in Figure 1 are consistent with the current generator theory. At first, when the injected particles traveled toward the inner magnetosphere, they were adiabatically energized in order to conserve the first adiabatic invariant. At the geosynchronous orbit, they may not have enough energy to depress the magnetic field. As they moved closer to the plasmapause, these particles were energized enough and could depress the magnetic field according

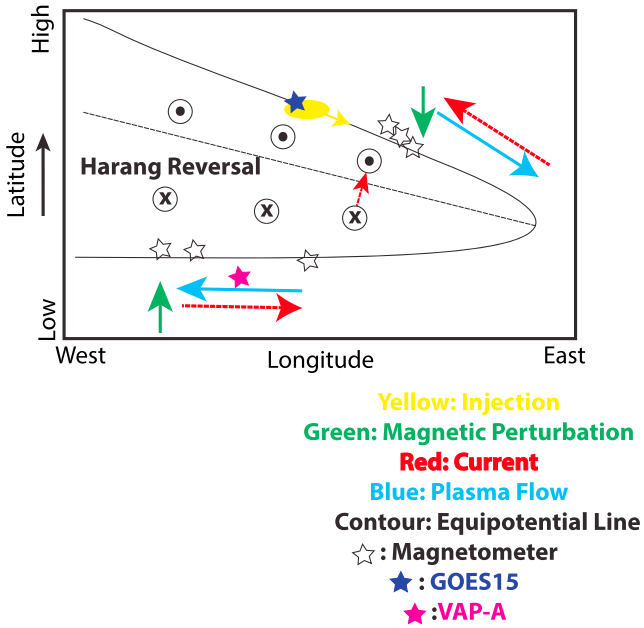

Figure 8. A schematic diagram of the convection flows, field-aligned currents, and magnetic perturbations near the Harang reversal. GOES = Geostationary Operational Environmental Satellite; VAP = Van Allen Probes.

to the diamagnetic effect (Gurgiolo et al., 1979; He, Chen, et al., 2017; Xia et al., 2017; Xiong et al., 2017). The magnetic dip in the inner magnetosphere is important for both the generation of butterfly PADs of electrons (Xiong et al., 2017) and electromagnetic ion cyclotron wave (He, Chen, et al., 2017; Remya et al., 2018). The magnetic field dip led to the decreasing of the energetic electron flux (Figure 1e) due to conservation of the first adiabatic invariant of electrons, consistent with earlier observations (He, Chen, et al., 2017). In this case, butterfly PADs were also observed by VAP-A at the energy of 31 keV (not shown).

We further tested the diamagnetic properties in the SAPS region. We first used the TS05 magnetic field magnitude minus 48 nT to fit the general trend of magnetic field ignoring the magnetic dip. Then this magnetic field was compared with the observed magnetic field, which shows that the magnetic pressure decreased by ~17 nPa at the center of magnetic dip and SAPS peak. The increase of the ion plasma pressure was about 12 nPa with contributions from both HOPE and MagEIS ($\Delta P_{\mathrm{HOPE}} + \Delta P_{\mathrm{MagEIS}} = 7 + 5$ nPa). This was quantitatively similar to the magnetic pressure decrease. Therefore, the magnetic field dip can be explained by the particle injections and the diamagnetic effects. This also shows that the injected particles can make a large contribution to the storm time ring current, as shown in Gkioulidou et al. (2014). Another interesting point is that this injection was observed to enter the inner magnetosphere at ~20 MLT and no injection was observed closer to the midnight sector. Therefore, this injection might be related with dynamics near the magnetopause flank, such as Kelvin-Helmholtz instability (Henderson, 2013). However, the exact source of the particle injection is out of the scope of this paper.

When a plasma pressure peak was generated in the inner magnetosphere, together with the gradient of the flux tube volume, a pair of Region 2 sense FACs can be generated near the edges of this dip (Figure 9), according to the Vasyliunas equation. In addition, this region was between the inner boundaries of ion and electron plasma sheets, and thus, the region where the downward FAC flows into in the ionosphere was of low conductivity. When the downward FAC closed poleward through the Pederson current and the upward Region 1 sense FAC, the electric field needed to increase to maintain current continuity. The above scenario explains the large poleward electric field in the ionosphere and radially outward electric field in the magnetosphere.

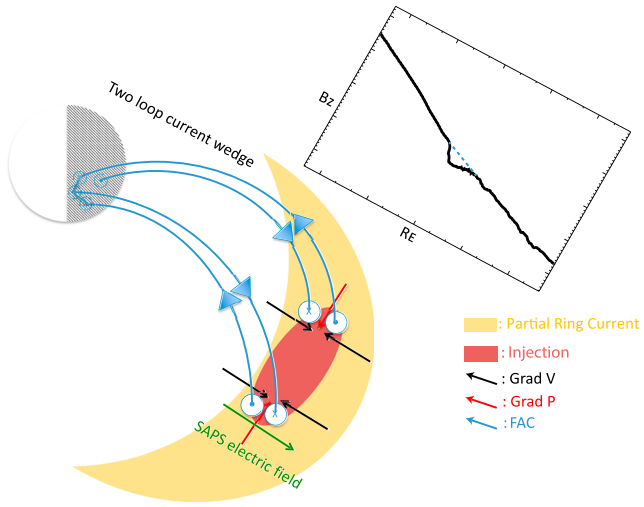

Figure 9. A schematic diagram of the formation of 2LCW and SAPS in the inner magnetosphere. SAPS = subauroral polarization streams; VAP = Van Allen Probes.

The results above lead to the schematic diagram of the formation of SAPS given in Figure 9. During geomagnetic storm time, a partial ring current develops due to the enhanced convection. The gradient of plasma thermal pressure in partial ring current and the gradient of the flux tube volume can generate the Region 2 FACs and thus SAPS (Anderson et al., 1993; Southwood & Wolf, 1978). This LS-SAPS should have a spatial scale comparable with the partial ring current and can extend several hours of magnetic local time. However, when a localized injection entering the inner magnetosphere and merging into the preexisting partial ring current, a localized pressure peak should form. At the same time, due to the diamagnetic effect, a local magnetic field dip can develop at the same location. The gradient of the flux tube volume points toward the local magnetic minimum. Therefore, the perturbed plasma pressure gradient and the flux tube volume gradient give rise to two pairs of FACs. The duskside pair is the Region 2 sense downward FACs close to the Earth and Region 1 sense upward FACs further away from the Earth. The other pair closer to midnight would have opposite polarity. These two pairs of FACs thus comprise a two-loop current wedge (2LCW). In duskside ionosphere, the Region 2 sense FACs close through poleward Pederson current and

then upward Region 1 sense FACs. This Pederson current flows in a low-conductivity region equatorward of the electron precipitation boundary and thus leads to a large poleward electric field, that is, SAPS electric field. Meanwhile, these FACs pairs superpose on top of the large-scale FAC systems near the equatorward edge of the aurora oval. This 2LCW can also explain the magnetic dip in the MGSE *x* direction. At the dusk-side, the MGSE Bx component can be considered westward. Both the downward FAC earthward of the dip and upward FAC further away from the dip can generate an eastward magnetic disturbance and thus reduce the Bx component in the MGSE coordinates. Note that this 2LCW should be differentiated against the 2L substorm current wedge. The latter is formed after substorm ons et although the formed FACs have similar polarities. In addition, no local magnetic field dip is invoked in the 2L substorm current wedge scenario. This mechanism can also be applied to LS-SAPS: The spatial scale of the SAPS depends on the scale of the particle injection. Injections can have variable scales from less than 1 hr in magnetic local time, for example, in this event, to 3 hr in magnetic local time in substorm injections, to the whole nightside during sawtooth-type injections (Arnoldy & Moore, 1983; Clauer et al., 2006; McPherron, 2015). Thus, the scale size of the SAPS enhancement should be directly related with the scale size of injections.

Auroral streamers in the ionosphere have been proposed to be the corresponding signature of flow bursts in the equatorial magnetosphere or injections when flow bursts reach the geosynchronous orbit (Forsyth et al., 2008; Henderson et al., 1998; Nakamura et al., 2001; Sergeev et al., 1999; Zou, Lyons, Wang, et al., 2009). Gallardo-Lacourt et al. (2017) showed that 98% streamers reaching equatorward boundary of the auroral oval are associated with SAPS and there is a strong correlation between the duration of SAPS and streamers. Nishimura et al. (2011) showed that not all streamers can lead to substorm onset. Thus, it is reasonable to infer that substorm onset is not necessary for streamers or particle injections and thus SAPS. Enhanced auroral activity was indeed observed during the first equatorward flow and SAPS enhancement, but it was not observed during the second case. This is very likely because the flow burst was observed by SuperDARN beams looking west of the ASI, and thus, the corresponding aurora activity is out of the field of view of the ASI.

Dispersionless particle injections are often observed during substorms right at or slightly after the substorm onset and have been used as a reliable substorm onset indicator. However, injections and substorms do not have a one-to-one correspondence (e.g., Angelopoulos et al., 1992; Gkioulidou et al., 2014). Sergeev et al. (1990) showed that injections can occur during steady convection time in addition to substorm time. This also suggests that substorm onset may not be necessary for injections and thus the formation of SAPS. Instead, SAPS can be generated directly by particle injections.

4. Summary and Conclusions

In this study, we performed a detailed case study of SAPS during the storm recovery phase on 18 May 2013 using conjugate VAP and SuperDARN as well as other complementary instruments. Energetic ion injections, energetic electron flux decrease, and local magnetic field dip were observed at the same time as the SAPS electric field by VAP-A deep in the inner magnetosphere at 3.5 R_E. The formation mechanism of the SAPS is suggested to be due to energetic particle injection together with the magnetic field distortion due to the injected particles' diamagnetic effect, which can generate a localized 2LCW with SAPS on its western side. SAPS is also shown to be part of the equatorward boundary of the Harang reversal, which started to develop before the substorm onset. Considering the correspondence between substorms and injections is not one to one, we suggest that SAPS can be generated directly due to particle injections induced pressure and flux tube volume gradients, no matter whether these injections are directly related with a substorm onset or not.

Acknowledgments
We acknowledge NSF AGS1342968 and NASA NNX14AF31G for supporting the work at the University of Michigan. Processing and analysis of the HOPE and MagEIS data was supported by Energetic Particle, Composition, and Thermal Plasma (RBSP-ECT) investigation funded under NASA Prime contract NAS5-01072. All RBSP-ECT data are publicly available at the Web site (http://www.RBSP-ect.lanl.gov/). We acknowledge the Van Allen Probe EMFISIS and EFW teams for data usage. The EMFISIS and EFW data used in the study are obtained from the websites (http://emfisis.physics.uiowa.edu/ and http://www.space.umn.edu/rbspefw-data/ respectively). We appreciate the discussion with S. Claudepierre about the MagEIS data. We thank GOES, SuperDARN, and SuperMAG team for high-quality data. SuperDARN and SuperMAG data are from the Web sites (https://www.ngdc.noaa.gov/stp/satellite/goes/; http://vt.superdarn.org/ and http://supermag.jhuapl.edu/ respectively). The OMNI data are available at CDAWeb. The aurora image files from ASI at Saskatoon can be found at the Web site (https://deepblue.lib.umich.edu/data/concern/generic_works/hq37vp515?locale=en).

References

Anderson, P. C. (2004). Subauroral electric fields and magnetospheric convection during the April, 2002 geomagnetic storms. *Geophysical Research Letters*, *31*, L11801. https://doi.org/10.1029/2004GL019588

Anderson, P. C., Carpenter, D. L., Tsuruda, K., Mukai, T., & Rich, F. J. (2001). Multisatellite observations of rapid subauroral ion drifts (SAID). *Journal of Geophysical Research*, *106*(A12), 29,585–29,600. https://doi.org/10.1029/2001JA000128

Anderson, P. C., Hanson, W. B., Heelis, R. A., Craven, J. D., Baker, D. N., & Frank, L. A. (1993). A proposed production model of rapid subauroral ion drifts and their relationship to substorm evolution. *Journal of Geophysical Research*, *98*(92), 6069–6078. https://doi.org/10.1029/92JA01975

Anderson, P. C., Heelis, R. A., & Hanson, W. B. (1991). The ionospheric signatures of rapid subauroral ion drifts. *Journal of Geophysical Research*, *96*(90), 5785–5792. https://doi.org/10.1029/90JA02651

Angelopoulos, V., Baumjohann, W., Kennel, C. F., Coroniti, F. V., Kivelson, M. G., Pellat, R., et al. (1992). Bursty bulk flows in the inner central plasma sheet. *Journal of Geophysical Research*, *97*(A4), 4027–4039. https://doi.org/10.1029/91JA02701

Arnoldy, R. L., & Moore, T. E. (1983). Longitudinal structure of substorm injections at synchronous orbit. *Journal of Geophysical Research*, *88*(A8), 6213–6220.

Banks, P. M., & Yasuhara, F. (1978). Electric fields and conductivity in the nighttime E-region. *Geophysical Research Letters*, *5*(12), 1047–1050.

Blake, J. B., Carranza, P. A., Claudepierre, S. G., Clemmons, J. H., Crain, W. R., Dotan, Y., et al. (2014). The Magnetic Electron Ion Spectrometer (MagEIS) instruments aboard the Radiation Belt Storm Probes (RBSP) spacecraft. *The Van Allen Probes Mission*, *9781489974*, 383–421. https://doi.org/10.1007/978-1-4899-7433-4-12

Burke, W. J., Rich, F. J., De, O., Beaujardiere, L., Huang, C. Y., & Wilson, G. R. (2000). Ionospheric disturbances observed by DMSP at middle to low latitudes during the magnetic storm of June 4-6. *Journal of Geophysical Research*, *105*(A8), 18,391–18,405.

Buzulukova, N., Fok, M.-C., Pulkkinen, A., Kuznetsova, M., Moore, T. E., Glocer, A., et al. (2010). Dynamics of ring current and electric fields in the inner magnetosphere during disturbed periods: CRCM-BATS-R-US coupled model. *Journal of Geophysical Research*, *115*, A05210. https://doi.org/10.1029/2009JA014621

Califf, S., Li, X., Wolf, R. A., Zhao, H., Jaynes, A. N., Wilder, F. D., et al. (2016). Large-amplitude electric fields in the inner magnetosphere: Van Allen Probes observations of subauroral polarization streams. *Journal of Geophysical Research: Space Physics*, *121*, 5294–5306. https://doi.org/10.1002/2015JA022252

Clauer, C. R., Cai, X., Welling, D., DeJong, A., & Henderson, M. G. (2006). Characterizing the 18 April 2002 storm-time sawtooth events using ground magnetic data. *Journal of Geophysical Research*, *111*, A04S90. https://doi.org/10.1029/2005JA011099

Clausen, L. B. N., Baker, J. B. H., Ruohoniemi, J. M., Greenwald, R. A., Thomas, E. G., Shepherd, S. G., et al. (2012). Large-scale observations of a subauroral polarization stream by midlatitude SuperDARN radars: Instantaneous longitudinal velocity variations. *Journal of Geophysical Research*, *117*, A05306. https://doi.org/10.1029/2011JA017232

De Keyser, J. (1999). Formation and evolution of subauroral ion drifts in the course of a substorm. *Journal of Geophysical Research*, *104*, 339–349.

Erickson, P. J., Beroz, F., & Miskin, M. Z. (2011). Statistical characterization of the American sector subauroral polarization stream using incoherent scatter radar. *Journal of Geophysical Research*, *116*, A00J21. https://doi.org/10.1029/2010JA015738

Forsyth, C., Lester, M., Cowley, S. W. H., Dandouras, I., Fazakerley, A. N., Fear, R. C., et al. (2008). Observed tail current systems associated with bursty bulk flows and auroral streamers during a period of multiple substorms. *Annales Geophysicae*, *26*(1), 167–184. https://doi.org/10.5194/angeo-26-167-2008

Foster, J. C., & Vo, H. B. (2002). Average characteristics and activity dependence of the subauroral polarization stream. *Journal of Geophysical Research*, *107*(A12), 1475. https://doi.org/10.1029/2002JA009409

Funsten, H. O., Skoug, R. M., Guthrie, A. A., MacDonald, E. A., Baldonado, J. R., Harper, R. W., et al. (2014). Helium, Oxygen, Proton, and Electron (HOPE) mass spectrometer for the Radiation Belt Storm Probes mission. *The Van Allen Probes Mission*, *179*, 423–484. https://doi.org/10.1007/978-1-4899-7433-4-13

Gallardo-Lacourt, B., Nishimura, Y., Lyons, L. R., Mishin, E. V., Ruohoniemi, J. M., Donovan, E. F., et al. (2017). Influence of auroral streamers on rapid evolution of ionospheric SAPS flows. *Journal of Geophysical Research: Space Physics*, *122*, 12,406–12,420. https://doi.org/10.1002/2017JA024198

Gallardo-Lacourt, B., Nishimura, Y., Lyons, L. R., Zou, S., Angelopoulos, V., Donovan, E., et al. (2014). Coordinated SuperDARN THEMIS ASI observations of mesoscale flow bursts associated with auroral streamers. *Journal of Geophysical Research: Space Physics*, *119*, 142–150. https://doi.org/10.1002/2013JA019245

Gjerloev, J. W. (2012). The SuperMAG data processing technique. *Journal of Geophysical Research*, *117*, A09213. https://doi.org/10.1029/2012JA017683

Gkioulidou, M., Ukhorskiy, A. Y., Mitchell, D. G., Sotirelis, T., Mauk, B. H., & Lanzerotti, L. J. (2014). The role of small-scale ion injections in the buildup of Earth's ring current pressure: Van Allen Probes observations of the 17 March 2013 storm. *Journal of Geophysical Research: Space Physics*, *119*, 7327–7342. https://doi.org/10.1002/2014JA020096

Gurgiolo, C., Lin, C. S., Mauk, B., Parks, G. K., & Mcilwain, C. (1979). Plasma injection and diamagnetism. *Journal of Geophysical Research*, *84*(8), 2049–2056.

He, Z., Chen, L., Zhu, H., Xia, Z., Reeves, G. D., Xiong, Y., et al. (2017). Multiple-satellite observation of magnetic dip event during the substorm on 10 October 2013. *Geophysical Research Letters*, *44*, 9167–9175. https://doi.org/10.1002/2017GL074869

He, F., Zhang, X.-X., Wang, W., Liu, L., Ren, Z.-P., Yue, X., et al. (2018). Large-scale structure of subauroral polarization streams during the main phase of a severe geomagnetic storm. *Journal of Geophysical Research: Space Physics*, *123*, 2964–2973. https://doi.org/10.1002/2018JA025234

He, F., Zhang, X.-X., Wang, W., & Wan, W. (2017). Different evolution patterns of subauroral polarization streams (SAPS) during intense storms and quiet-time substorms. *Geophysical Research Letters*, *44*, 10,796–10,804. https://doi.org/10.1002/2017GL075449

Heelis, R. A., Bailey, G. J., Sellek, R., Moffett, R. J., & Jenkins, B. (1993). Field-aligned drifts in subauroral ion drift events. *Journal of Geophysical Research*, *98*(A12), 21,493–21,499. https://doi.org/10.1029/93JA02209

Henderson, M. G. (2013). Auroral substorms, poleward boundary activations, auroral streamers, omega bands, and onset precursor activity. *Auroral Phenomenology and Magnetospheric Processes: Earth and Other Planets*, *197*, 39–54. https://doi.org/10.1029/2011GM001165

Henderson, M. G., Reeves, G. D., & Murphree, J. S. (1998). Are north-south aligned auroral structures an ionospheric manifestation of bursty bulk flows? *Geophysical Research Letters*, *25*(19), 3737–3740. https://doi.org/10.1029/98GL02692

Huang, C. S., & Foster, J. C. (2007). Correlation of the subauroral polarization streams (SAPS) with the Dst index during severe magnetic storms. *Journal of Geophysical Research*, *112*, A11302. https://doi.org/10.1029/2007JA012584

Karlsson, T., Marklund, G. T., Blomberg, L. G., & Mälkki, A. (1998). Subauroral electric fields observed by the Freja satellite: A statistical study. *Journal of Geophysical Research*, *103*(1), 4327–4342. https://doi.org/10.1029/97JA00333

Kim, K. H., Mozer, F. S., Lee, D. H., & Jin, H. (2010). Large electric field at the nightside plasmapause observed by the Polar spacecraft. *Journal of Geophysical Research*, *115*(7), A07219. https://doi.org/10.1029/2010JA015439

Kletzing, C. A., Kurth, W. S., Acuna, M., MacDowall, R. J., Torbert, R. B., Averkamp, T., et al. (2014). The Electric and Magnetic Field Instrument suite and Integrated Science (EMFISIS) on RBSP. *The Van Allen Probes Mission*, *179*, 127–181. https://doi.org/10.1007/978-1-4899-7433-4-5

Kunduri, B. S. R., Baker, J. B. H., Ruohoniemi, J. M., Thomas, E. G., Shepherd, S. G., & Sterne, K. T. (2017). Statistical characterization of the large-scale structure of the subauroral polarization stream. *Journal of Geophysical Research: Space Physics*, *122*, 6035–6048. https://doi.org/10.1002/2017JA024131

Lejosne, S., & Mozer, F. S. (2017). Sub-Auroral Polarization Stream (SAPS) duration as determined from Van Allen Probe successive electric drift measurements. *Geophysical Research Letters*, *44*, 9134–9141. https://doi.org/10.1002/2017GL074985

Lühr, H., Park, J., Gjerloev, J. W., Rauberg, J., Michaelis, I., Merayo, J. M., & Brauer, P. (2015). Field-aligned currents' scale analysis performed with the Swarm constellation. *Geophysical Research Letters*, *42*, 1–8. https://doi.org/10.1002/2014GL062453

Makarevich, R. A., Kellerman, A. C., Bogdanova, Y. V., & Koustov, A. V. (2009). Time evolution of the subauroral electric fields: A case study during a sequence of two substorms. *Journal of Geophysical Research*, *114*, A04312. https://doi.org/10.1029/2008JA013944

Makarevich, R. A., Kellerman, A. C., Devlin, J. C., Ye, H., Lyons, L. R., & Nishimura, Y. (2011). SAPS intensification during substorm recovery: A multi-instrument case study. *Journal of Geophysical Research*, *116*, A11311. https://doi.org/10.1029/2011JA016916

Mauk, B. H., Fox, N. J., Kanekal, S. G., Kessel, R. L., Sibeck, D. G., & Ukhorskiy, A. (2014). Science objectives and rationale for the Radiation Belt Storm Probes mission. *The Van Allen Probes Mission*, *179*, 3–27. https://doi.org/10.1007/978-1-4899-7433-4-2

McGranaghan, R. M., Mannucci, A. J., & Forsyth, C. (2017). A comprehensive analysis of multiscale field-aligned currents: Characteristics, controlling parameters, and relationships. *Journal of Geophysical Research: Space Physics*, *122*, 11,931–11,960. https://doi.org/10.1002/2017JA024742

McPherron, R. L. (2015). Earth's magnetotail, *Magnetotails in the solar system* (pp. 61–84). Washington, DC: American Geophysical Union (AGU).

Mishin, E. V. (2013). Interaction of substorm injections with the subauroral geospace: 1. Multispacecraft observations of SAID. *Journal of Geophysical Research: Space Physics*, *118*, 5782–5796. https://doi.org/10.1002/jgra.50548

Mishin, E. V. (2016). SAPS onset timing during substorms and the westward traveling surge. *Geophysical Research Letters*, *43*, 6687–6693. https://doi.org/10.1002/2016GL069693

Mishin, E. V., & Puhl-Quinn, P. A. (2007). SAID: Plasmaspheric short circuit of substorm injections. *Geophysical Research Letters*, *34*, L24101. https://doi.org/10.1029/2007GL031925

Moore, T. E., Arnoldy, R. L., Feynman, J., & Hardy, D. A. (1981). Propagating substorm injection fronts. *Journal of Geophysical Research*, *86*(A8), 6713–6726.

Nakamura, R., Baurnjohann, W., Brittnacher, M., Sergeev, VA, Kubyshkina, M., Mukai, T., & Liou, K. (2001). Onset timing and foot point location Brige-Hopfield long filter. *Journal of Geophysical Research*, *106*, 777–789.

Nishimura, Y., Lyons, L. R., Angelopoulos, V., Kikuchi, T., Zou, S., & Mende, S. B. (2011). Relations between multiple auroral streamers, pre-onset thin arc formation, and substorm auroral onset. *Journal of Geophysical Research*, *116*, A09214. https://doi.org/10.1029/2011JA016768

Nishimura, Y., Wygant, J., Ono, T., Iizima, M., Kumamoto, A., Brautigam, D., & Friedel, R. (2008). SAPS measurements around the magnetic equator by CRRES. *Geophysical Research Letters*, *35*, L10104. https://doi.org/10.1029/2008GL033970

Oksavik, K., Greenwald, R. A., Ruohoniemi, J. M., Hairston, M. R., Paxton, L. J., Baker, J. B. H., et al. (2006). First observations of the temporal/spatial variation of the sub-auroral polarization stream from the SuperDARN Wallops HF radar. *Geophysical Research Letters*, *33*, L12104. https://doi.org/10.1029/2006GL026256

Puhl-Quinn, P. A., Matsui, H., Mishin, E., Mouikis, C., Kistler, L., Khotyaintsev, Y., et al. (2007). Cluster and DMSP observations of SAID electric fields. *Journal of Geophysical Research*, *112*, A05219. https://doi.org/10.1029/2006JA012065

Reeves, G. D., Henderson, M. G., McLachlan, P. S., Belian, R. D., Friedel, R. H. W., & Korth, A. (1996). Radial propagation of substorm injections. In *International conference on substorms*, pp. 579. Vol. 389.

Remya, B., Sibeck, D. G., Halford, A. J., Murphy, K. R., Reeves, G. D., Singer, H. J., et al. (2018). Ion injection triggered EMIC waves in the Earth's magnetosphere. *Journal of Geophysical Research: Space Physics*, *123*, 4921–4938. https://doi.org/10.1029/2018JA025354

Schunk, R. W., Banks, P. M., & Raitt, W. J. (1976). Effects of electric fields and other processes upon the nighttime high-latitude F layer. *Journal of Geophysical Research*, *81*(19), 3271–3282. https://doi.org/10.1029/JA081i019p03271

Sergeev, V. A., Aulamo, O. A., Pellinen, R. J., Vallinkoski, M. K., Bosinger, T., Cattell, C. A., et al. (1990). Non-substorm transient injection events. *Planetary and Space Science*, *38*(2), 231–239.

Sergeev, V. A., Liou, K., Meng, C. I., Newell, P. T., Brittnacher, M., Parks, G., & Reeves, G. D. (1999). Development of auroral streamers in association with localized impulsive injections to the inner magnetotail. *Geophysical Research Letters*, *26*(3), 417–420. https://doi.org/10.1029/1998GL900311

Southwood, D. J., & Wolf, R. A. (1978). An assessment of the role of precipitation in magnetospheric convection. *Journal of Geophysical Research*, *83*(A11), 5227–5232. https://doi.org/10.1029/JA083iA11p05227

Tsyganenko, N. A., & Sitnov, M. I. (2005). Modeling the dynamics of the inner magnetosphere during strong geomagnetic storms. *Journal of Geophysical Research*, *110*, A03208. https://doi.org/10.1029/2004JA010798

Vasyliunas, V. (1970). Mathematical models of magnetospheric convection and its coupling to the ionosphere (Vol. 17).

Wang, H., & Lühr, H. (2011). The efficiency of mechanisms driving subauroral polarization streams (SAPS). *Annales Geophysicae*, *29*(7), 1277–1286. https://doi.org/10.5194/angeo-29-1277-2011

Wang, H., Ridley, A. J., Lühr, H., Liemohn, M. W., & Ma, S. Y. (2008). Statistical study of the subauroral polarization stream: Its dependence on the cross-polar cap potential and subauroral conductance. *Journal of Geophysical Research*, *113*, A12311. https://doi.org/10.1029/2008JA013529

Wygant, J. R., Bonnell, J. W., Goetz, K., Ergun, R. E., Mozer, F. S., Bale, S. D., et al. (2014). *The Electric Field and Waves Instruments on the Radiation Belt Storm Probes mission* (Vol. 179, pp. 1–4). https://doi.org/10.1029/2008JA013529

Xia, Z., Chen, L., Zheng, L., & Chan, A. A. (2017). Eigenmode analysis of compressional poloidal modes in a self-consistent magnetic field. *Journal of Geophysical Research: Space Physics*, *122*, 10,369–10,381. https://doi.org/10.1002/2017JA024376

Xiong, Y., Chen, L., Xie, L., Fu, S., Xia, Z., & Pu, Z. (2017). Relativistic electron's butterfly pitch angle distribution modulated by localized background magnetic field perturbation driven by hot ring current ions. *Geophysical Research Letters*, *44*, 4393–4400. https://doi.org/10.1002/2017GL072558

Yu, Y., Jordanova, V., Zou, S., Heelis, R., Ruohoniemi, M., & Wygant, J. (2015). Modeling subauroral polarization streams during the 17 March 2013 storm. *Journal of Geophysical Research: Space Physics*, *120*, 1738–1750. https://doi.org/10.1002/2014JA020371

Zhao, H., Li, X., Baker, D. N., Fennell, J. F., Blake, J. B., Larsen, B. A., et al. (2015). The evolution of ring current ion energy density and energy content during geomagnetic storms based on Van Allen Probes measurements. *Journal of Geophysical Research: Space Physics*, *120*, 7493–7511. https://doi.org/10.1002/2015JA021533

Zou, S., Lyons, L. R., Nicolls, M. J., Heinselman, C. J., & Mende, S. B. (2009). Nightside ionospheric electrodynamics associated with substorms: PFISR and THEMIS ASI observations. *Journal of Geophysical Research*, *114*, A12301. https://doi.org/10.1029/2009JA014259

Zou, S., Lyons, L. R., & Nishimura, Y. (2012). Mutual evolution of aurora and ionospheric electrodynamic features near the Harang reversal during substorms. *Geophysical Monograph Series*, *197*, 159–169. https://doi.org/10.1029/2011GM001163

Zou, S., Lyons, L. R., Wang, C. P., Boudouridis, A., Ruohoniemi, J. M., Anderson, P. C., et al. (2009). On the coupling between the Harang reversal evolution and substorm dynamics: A synthesis of SuperDARN, DMSP, and IMAGE observations. *Journal of Geophysical Research*, *114*, A01205. https://doi.org/10.1029/2008JA013449